Journal of The Electrochemical Society, **150** (12) G838-G842 (2003)
0013-4651/2003/150(12)/G838/5/$7.00 © The Electrochemical Society, Inc.

Ramp-Rate Effects on Transient Enhanced Diffusion and Dopant Activation

M. Y. L. Jung, R. Gunawan, R. D. Braatz, and E. G. Seebauer[z]

Department of Chemical Engineering, University of Illinois, Urbana, Illinois 61801, USA

Use of high ramp rates (>400°C/s) in rapid thermal annealing after ion implantation leads to experimentally observed improvements in junction depth and the reverse narrow-channel effect. However, a straightforward explanation for this effect has been lacking. Via modeling, we find that increasing the heating rate permits clusters with dissociation energies lower than the maximum of 3.5-3.7 eV to survive to higher temperatures. This improved survival delays the increase in Si interstitial concentrations near the top of an annealing spike, which decreases the profile spreading.
© 2003 The Electrochemical Society. [DOI: 10.1149/1.1627354] All rights reserved.

Manuscript submitted November 5, 2002; revised manuscript received July 1, 2003. Available electronically November 3, 2003.

Forming extremely shallow pn junctions in Si-based microelectronic logic devices is becoming increasingly critical as device dimensions continue to diminish. Ion implantation technology for junction formation is limited in part by transient enhanced diffusion (TED) of dopants during postimplant rapid thermal annealing (RTA), often leading to significant spreading of the original dopant profile.

Several years ago there appeared experimental evidence that increasing the ramp rate, β, of the "spike" profile conventionally used for annealing up to 400°C/s or more, could improve junction depth X_j, leakage current, and other device metrics.[1] While immediately subsequent literature seemed divided over the efficacy of this procedure,[2,3] the debate probably originated from varying conditions of preamorphization, implant energy and dose, and other factors. Very recent results[4] using specialized techniques for achieving $\beta \sim 10^4$°C/s have confirmed the improvements originally claimed. However, to our knowledge, no straightforward and reliable explanation for the improvement has been published. Such understanding is important for predicting what will happen as technological innovations push heating rates up to very large values, as in laser annealing and related techniques.[4]

This paper seeks to explain the benefits of fast ramping through modeling that employs a firmly grounded set of rate parameters developed in our laboratory[5,6] by maximum likelihood (ML) estimation together with an analytical model[7] that describes the size dependence of the dissociation energies for interstitial clusters.

Comparison of Simulations and Experiment

Calculations were performed using the profile simulator FLOOPS 2000.[a,8] This simulator solves the coupled mass balance equations for interstitials, vacancies, and clusters. These equations have the general form for species j

$$\frac{\partial N_j}{\partial t} = -\frac{\partial J_j}{\partial x} + G_j \qquad [1]$$

where N_j denotes concentration and G a net generation rate. The flux J comprises terms due to both diffusion and drift in response to electric fields. The electric fields are obtained by solution of Poisson's equation. FLOOPS was implemented with the rate expressions and parameters shown in Tables I and II together with no-flux surface boundary conditions for all species[b,9] and no surface band bending. Concentrations of charged interstitial B and Si species were computed according to Fermi statistics as described elsewhere.[10]

Due to the number of cluster species that can be tracked by FLOOPS 2000, cluster sizes were limited to four atoms for pure B and Si clusters and five for mixed B-Si clusters. The entire distribution of cluster dissociation energies has been captured in the present model by equating the size 5 dissociation energy to that of the large interstitial clusters (~3.5-3.7 eV). That model telescoped the entire cluster dissociation cascade into a computationally manageable set of events. According to a detailed parameter sensitivity analysis that appears elsewhere,[6] the junction depth and degree of boron activation were not sensitive to the dissociation energy of size 5 clusters, but rather to the dissociation of intermediate-sized clusters. This finding, together with experimental observations from spike RTA of sub-keV implanted wafers indicating that large clusters do not form,[11] suggests that the limitation on cluster size does not impose serious restrictions on physical interpretations drawn from the simulation.

Initial conditions on the profiles for Si_i were set to track the local concentration of total boron. For total boron we employed experimental as-implanted profiles as initial conditions, with a fixed fraction of one-fifth of the total boron in substitutional sites, in accord with the suggestion of Caturla *et al.*[12] and Kobayashi *et al.*[13] Figure 1 shows a typical annealing program employed.

Figure 2 shows the experimental profiles; junction depths decreased from 63 to 54 to 49 nm for heating rates of 25, 150, and 350°C/s, respectively. Downey *et al.* obtained similar results for a comparable set of conditions.[14]

Simulation profiles also appear in Fig. 2, with junction depths decreasing from 75 to 53 to 50 nm for increasing heating rates of 25, 150, and 350°C/s, respectively. Most of the decrease took place at the lower heating rates; increasing β above 150°C/s provided little additional improvement. Mannino *et al.*[15] also reported diminishing improvement above 100°C/s using delta-doped B superlattices, while Agarwal *et al.*[16] showed no improvement of the junction depth above 150°C/s through simulations. Figure 3 shows this effect for the change in the junction depth as well as a degree of boron electrical activation (*i.e.*, fraction of boron in substitutional sites) integrated over the profiles. Activation decreased with increasing β. As with junction depth, most of the change took place at lower heating rates.

Although the simulations capture the qualitative trends and many quantitative features of the profiles, there is a nontrivial quantitative discrepancy between the simulation and experimental profiles for $\beta = 25$°C/s. We speculate that the difference arises from our use of a perfectly reflecting surface boundary condition. This condition does not quite hold in reality;[17] some interstitials are absorbed at a free surface or Si/SiO_2 interface. Removal of Si interstitials is well known to reduce the degree of profile spreading, so the experimental profiles should exhibit less spreading than profiles simulated using a perfect-reflector boundary condition. The overestimation should be more pronounced for lower heating rates because Si interstitials in experiments have longer times to escape to the surface.

[z] E-mail: eseebaue@uiuc.edu

[a] Mark E. Law of the University of Florida and Al Tasch of the University of Texas/Austin.

[b] No-flux boundary conditions represent an approximation that suffer deficiencies as discussed in Ref. 17. However, in the regime of the simulations, the conclusions of this paper are insensitive to the details of these conditions.

Table I. Activation energies for interstitial diffusion and cluster association.

Reaction	Symbol[a]	Activation energy (eV)	Reference	Method[b]
B_i diffusion	E_{diff,B_i}	0.37 ± 0.04[c]	5	ML
Si_i diffusion	E_{diff,Si_i}	0.72 ± 0.03[c]	5	ML
$B_i + Si_s \rightarrow (B_s - Si_i)$	E_{ki}	0.50 ± 0.1	5	ML
$B_m - Si_n + B_i \rightarrow B_{m+1} - Si_n,\ n,m \geq 0$[d]	$E_{assoc,B}$	0.37 ± 0.04[e]	5	Assumed $= E_{diff,B_i}$
$B_m - Si_n + Si_i \rightarrow B_m - Si_{n+1},\ n,m \geq 0$[d]	E_{assoc}	0.72 ± 0.03[e]	5	Assumed $= E_{diff,Si_i}$

[a] For clarity in focus on cluster effects, the present work uses slightly different notation than related publications from this laboratory.[5] Where two symbols are given here, the latter symbol appears in Ref. 5.
[b] ML = Maximum likelihood estimation.
[c] The pre-exponential factor for this diffusion has been assumed to be 1×10^{-3} cm^2/s.[5]
[d] For $m \geq 1$, one of the boron atoms is presumed to be substitutional. Also, m and n must obey $m + n \geq 2$ and $m + n \leq 4$. Finally, if $n = 0$, then m is assumed to obey $m \leq 2$. (No pure boron clusters larger than dimers form.)
[e] The pre-exponential factor for this association reaction has been assumed to be 3×10^{-10} cm^2/s,[5] regardless of cluster size. Also, if two free Si interstitials recombine, the stochiometric factor of 2 has been neglected.

Explanation of Heating Rate Effects

In previous publications,[5,6] we showed that diffusion of boron observed in TED is most likely mediated by motion of free B_i (as proposed in early work[18,19]) rather than motion of small complexes such as $(B_s - Si_i)$ or $(B_s - B_i)$. In Ref. 7 we offered strong evidence that boron exchange with lattice sites (mediated by interstitial Si) is the primary mechanism by which motion of free B_i is hampered, as opposed to accretion onto nondissociated clusters. When this exchange mechanism dominates, boron moves while it is a free interstitial (slightly impeded by exchange with the $(B_s - Si_i)$ complex), but is rapidly immobilized when $(B_s - Si_i)$ releases Si_i. The trapped boron atom can move again only after lengthy periods of waiting for association with another free Si interstitial. The time constant describing this waiting period[7] is $(k_{assoc}[Si_i])^{-1}$, where k_{assoc} denotes the rate constant for the association reaction between B_s and Si_i. During the second or so that the temperature remains within about 50°C of the top of a 1050°C spike in conventional RTA, liberation can take place several hundred times. By defining t_{max} as a characteristic time over which the wafer remains near the peak temperature, the number of liberation events can be estimated from the ratio of t_{max} to the characteristic time $(k_{assoc}[Si_i])^{-1}$ for the association reaction. Then the degree of profile spreading can be estimated from Ref. 7

$$x^2 = \frac{6D_{diff,B_i}}{k_{ki}} k_{assoc}[Si_i] t_{max} \left(\frac{1 - b}{b} \right) \quad [2]$$

where k_{ki} and D_{diff,B_i} represent respectively the rate constant for kick-in and the diffusion coefficient for B_i hopping. The branching ratio b describing the pathways for the dissociation reaction of $(B_s\text{-}Si_i)$ to form B_i and Si_i is given by

$$b = \frac{r_{(B_s - Si_i) \rightarrow Si_i + B_s}}{r_{(B_s - Si_i) \rightarrow Si_i + B_s} + r_{(B_s - Si_i) \rightarrow B_i + Si}} \quad [3]$$

During heating, interstitial silicon is produced mainly by the dissociation of clusters. Because there is no lattice reservoir for Si_i equivalent to that for B_i (because the lattice holds primarily Si atoms), most Si_i diffuses rapidly over large distances. Thus, spatial

Table II. Activation energies for cluster dissociation.[a]

Composition	Cluster size	Species liberated	Symbol	Activation energy (eV)	Reference	Method[b]
Pure B	2	B	$E_{2,B}$	1.70 ± 0.07	6	ML
Pure Si	2	Si	E_2	1.41 ± 0.03	6	ML
	3	Si	E_3	2.2	6	Linear interpolation
	4	Si	E_4	3.0	6	Linear interpolation
	5	Si	E_{large}	3.7 ± 0.1	6	ML
Mixed B-Si	2[c]	B	$E_{2,mix\rightarrow B} = E_{ko}$	0.50	6	From dopant activation[d]
	2[e]	Si	$E_{2,mix\rightarrow Si} = E_{dis}$	0.59 ± 0.06	5	ML
	3	B	$E_{3,mix}$	2.2	6	Assumed$=E_3$
	3	Si	$E_{3,mix}$	2.2	6	Assumed$=E_3$
	4	B	$E_{4,mix}$	3.0	6	Assumed$=E_4$
	4	Si	$E_{4,mix}$	3.0	6	Assumed$=E_4$
	5	B	$E_{large,mix}$	3.5	22	DFT
	5	Si	$E_{large,mix}$	3.5	22	DFT

[a] All pre-exponential factors are assumed equal to 6×10^{12} s^{-1}.[5]
[b] ML = Maximum likelihood estimation.
[c] This represents the kick-out reaction $(B_s - Si_i) \rightarrow B_i + Si_s$.
[d] ML method in Ref. 5 yielded 1.05 eV. The value in the table is calculated from published data for dopant activation (equivalent to solid solubility) as discussed in text.
[e] This represents the dissociation reaction $(B_s - Si_i) \rightarrow B_s + Si_i$.

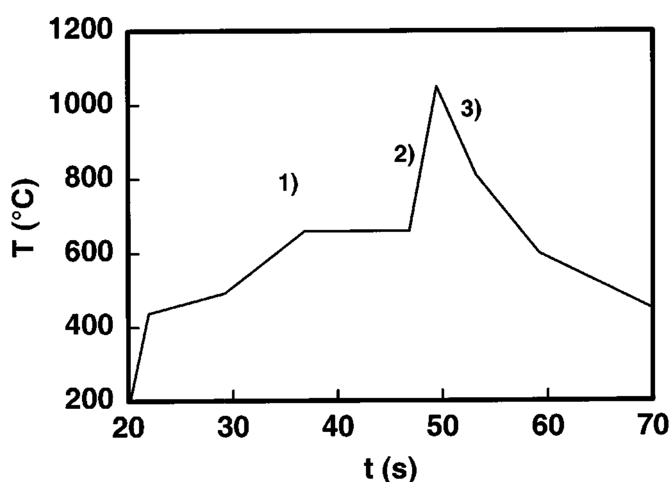

Figure 1. Typical temperature program for simulated spike anneals. (1) temperature stabilization between about 400 and 660°C, (2) main spike with β = 150°C/s, (3) maximum temperature T_M = 1050°C, and (4) radiative ramp-down, initial rate of 64°C/s. In simulations, β was varied between 25 and 350°C/s.

profiles for $[Si_i]$ are flat compared with most other species in the implanted system.[7] During the main spike, $[Si_i]$ rises dramatically throughout the profile because of (*i*) increasing release rates from clusters (due to the larger average number of Si atoms per cluster and the larger number of stoichiometric permutations of mixed clusters), and (*ii*) decreasing net capture rates due to the decreasing total number of clusters. The increase in $[Si_i]$ permits the profile spreading x in Eq. 2 to grow.

Clusters come in many sizes ranging up from two. The activation energy for cluster dissociation exhibits significant size dependence, as reviewed in Ref. 6. For example, initial dissociation events can have activation energies ranging from 1.4 eV for Si dimers up to 3.7 eV for large Si clusters. The number of dissociation pathways between these extremes is large if compositional and structural isomers including boron are taken into account. Therefore, it is plausible to describe these pathways using a nearly continuous distribution of dissociation energies. Whatever the cluster size, the dissociation rate constant exhibits a strong exponential variation with temperature. Thus, during a ramp, the clusters can be categorized as being in

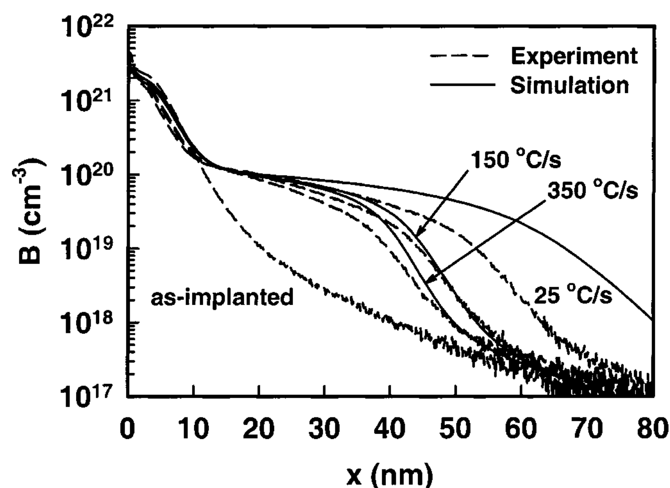

Figure 2. Experimental and simulated boron profiles as a function of heating rate. The wafers cooled largely by free radiation immediately after reaching T_{max}. The junction depth is defined as the distance from the surface at which the total boron concentration reaches 10^{18} atoms/cm^3.

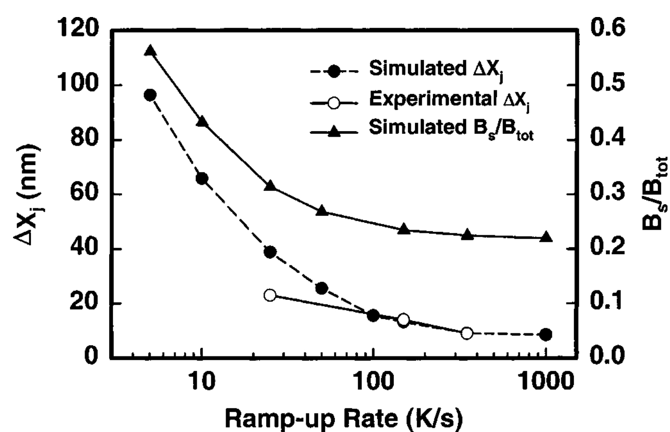

Figure 3. Simulated and experimental changes in junction depth as well as simulated changes in electrical activation (B_s/B_{tot}) for conditions corresponding to data in Fig. 1.

three classes: almost fully dissociated, presently dissociating, and not yet dissociated. At any given temperature, only the class in the "presently dissociating" class contributes significantly to interstitial release.

This kinetic situation has been treated extensively in the literature in the context of gas desorption from surfaces. Several assumptions are required to translate those results into a useful quantitative description in the present case. First, dissociation must occur in the equivalent of a single step. This assumption is satisfied because release of the first atom from a cluster has by far the highest activation energy, so that the subsequent dissolution cascade is very rapid. Second, interstitial reassociation with the most actively dissociating clusters must be neglected. Satisfaction of this assumption can be determined by simple arguments derived from the data of Tables I and II, and confirmed by the fact that the size 5 cluster concentration in simulations did not increase appreciably during the dissociation of smaller clusters. Third, the distribution of dissociation energies must be wider than 1.5 kT. Since kT ~ 0.1 eV at 1300 K and the distribution of dissociation energies has a standard deviation on the order of 1 eV, this condition is easily met. A clean, closed-form analytical expression can be obtained[20] connecting each temperature in a linear ramp with the dissociation energy E^* of the most active dissociating species

$$(E^*/kT - 1/2)\exp(E^*/kT - 1/2) = \nu T/\beta \qquad [4]$$

where ν is the pre-exponential factor for dissociation, which should typically lie near the Debye frequency and β is the heating rate. For simplified calculation of E^*, this transcendental expression can be replaced by the analytical expression[21]

$$E^*/kT = 1/2 + Y - \ln Y + (\ln Y)/Y - (2 - \ln Y)(\ln Y)/(2Y^2) \qquad [5]$$

where $Y \equiv \ln(\nu T/\beta)$. The approximation has negligible error the order of $[\ln Y/(Y)]^3$, which is 1.5×10^{-3} for a typical value of Y near 30.

Increasing the heating rate β raises the temperature at which clusters with a given value of E^* actively dissociate. If E^* is specified, the magnitude of this effect can be estimated in a local region about E^* by taking the derivative of Eq. 4 and rearranging to obtain

$$\frac{dT}{d\beta} = \frac{\frac{T}{\beta}\left(\frac{E^*}{kT} - \frac{1}{2}\right)}{\left(\frac{E^*}{kT} - \frac{1}{2}\right) + \frac{E^*}{kT}\left(\frac{E^*}{kT} + \frac{1}{2}\right)} \qquad [6]$$

If $E^*/kT \gg 1$, which is true during TED, this simplifies to

$$dT/d\beta = kT^2/\beta E^* \quad [7]$$

which makes the dependency on temperature and dissociation energy much clearer. For $E^* = 3.0$ eV and $\beta = 25$ K/s (where $T = 874°C = 1147$ K), Eq. 6 yields $dT/d\beta = 1.4$ K/(K/s). That is, raising the heating rate β by 1 K/s causes the temperature at which the clusters of dissociation energy E^* are most active to increase by 1.4 K.

Because $dT/d\beta$ depends upon β, the differential equation represented by Eq. 6 is more useful for practical calculations in integrated form. A particularly simple form can be obtained by recognizing that, for the range of kinetic parameters of interest in standard rapid thermal processing, E^*/kT typically lies near 30 (within about 5%). This result is quite general in many fields of kinetics. The numerical value of 30 follows primarily from the general magnitude of ν (near an atomic vibration frequency of 10^{12} s^{-1}) and β (within a few orders of magnitude 10 K/s). The weak dependence of E^*/kT on ν and β keeps E^*/kT in this vicinity over a surprisingly wide range of conditions. With this approximation, Eq. 6 can be integrated for constant E^* between two heating rates β_1 and β_2 to yield the following expression

$$T_2/T_1 \approx (\beta_2/\beta_1)^{1/32} \quad [8]$$

In the example just given, Eq. 8 predicts that the temperature where $E^* = 3.0$ eV dominates the dissociation rate should increase from 1147 K at $\beta = 25$ K/s to 1213 K = 941°C at $\beta = 150$ K/s. In fact, this result lies within one degree of the exact result given by Eq. 4.

Effects on profile spreading.—The above numerical example gives the key to understanding why increasing heating rate should reduce TED. Figure 4 shows concentrations of Si_i and clusters having size four (*i.e.*, pure Si and mixed B − Si) as a function of T for two heating rates, 25 and 150 K/s. Based on ML estimation, the size four clusters were assigned a dissociation energy of 3.0 eV.[6] Notice how the concentration of these clusters begins to decline substantially at roughly 875°C for $\beta = 25$ K/s, but is delayed to about 950°C for $\beta = 150$ K/s. Higher heating rates delay the dissociation even further.

Computational constraints[7] limit the size of the clusters that these simulations can employ to five. In light of these considerations, the results of Fig. 4 should not be interpreted to mean that there is something magical about size four clusters. The important point is that there exist clusters that dissociate with energies only slightly below the maximum dissociation energy of 3.5 to 3.7 eV that are characteristic of very large clusters. Near the top of the spike only large clusters with dissociation energies at or near 3.5 to 3.7 eV remain, and their fairly wide spacing permits many interstitials to roam freely before accreting onto them. Increasing β permits clusters with dissociation energies significantly lower than this level to survive to higher temperatures. This improved survival helps reduce $[Si_i]$ both by slowing the release of interstitials by cluster dissociation, and by increasing the net rate of interstitial accretion onto clusters. Figure 4 shows that the rise in concentration of Si_i is therefore delayed. This, coupled with the longer time a wafer spends near the peak temperature at lower heating rates, means that higher heating rates expose the diffusing profile to large concentrations of Si_i for less time, and therefore decrease the profile spreading as given by Eq. 2.

Increasing β brings diminishing returns (Fig. 3), especially as β begins to greatly exceed the initial cooling rate. Moreover, Fig. 4 also shows that, after the maximum temperature is reached, Si_i concentration follows temporal profiles that are largely independent of β. Thus, exposure of the profile to Si_i cannot be readily changed through variations in β alone, and profile spreading becomes limited by the cooling rate.

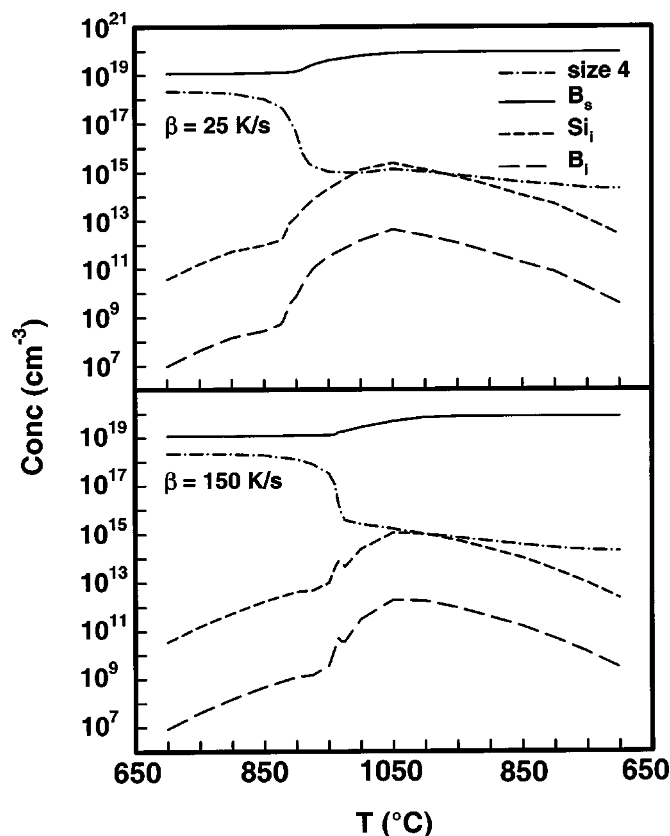

Figure 4. Concentrations of Si_i and clusters having size four (*i.e.*, pure Si and mixed B-Si) as a function of T for two heating rates in the simulations of Fig. 1. Concentrations are averaged over 10 to 40 nm in the bulk, corresponding to the region where most TED takes place. Qualitative behavior is the same throughout the profile. Concentration of B_i tracks that of Si_i but is roughly three orders of magnitude lower. Increasing the heating rate delays the dissociation of size four clusters from roughly 870°C to roughly 940°C, in accord with Eq. 4 and 5. The rise in concentration of Si_i is therefore delayed. This fact, coupled with the longer time a wafer spends near the peak temperature at lower heating rates, means that higher heating rates expose the diffusing profile to large concentrations of Si_i for less time.

Effects on dopant activation.—Boron becomes electrically active by entering lattice sites via the $(B_s - Si_i)$ complex and then releasing Si_i. As mentioned above, an individual boron atom moves through various lattice sites several hundred times near the spike maximum. The activation energies governing these exchanges are low, 0.5 to 0.6 eV,[5] meaning that the temperature dependence is small. However, as T decreases during cool-down, the rapidly declining release rate of interstitials from clusters, combined with the fast diffusion of Si interstitials to the surface or into the bulk, serves to decrease interstitial concentrations throughout the profile. Thus, the exchange rate of boron with lattice sites decreases correspondingly, because B_s must capture Si_i in order to escape the lattice. As shown in Fig. 4, $[Si_i]$ drops one to two orders of magnitude by 800°C, causing the time constant for B_s release to increase above one second. By this point, B_s has in effect frozen into the lattice at roughly the concentration it achieved near the top of the spike. The total number of boron atoms activated throughout the profile decreases as β increases mainly because the profile spreading decreases. Almost all boron that moves due to profile spreading is activated, so increased spreading merely removes boron from its inactive clustered form near the surface and moves it into active form deeper in the bulk. This effect explains most of the tradeoff between junction depth and boron activation that is well known and whose essence is captured in Fig. 3.

Acknowledgments

This work was supported by NSF (CTS 98-06329 and CTS 02-03237) and by Sematech.

References

1. S. Shishiguchi, A. Mineji, T. Hayashi, and S. Saito, in *Technical Digest for 1997 Symposium on VLSI Technology*, Vol. 7B, p. 89 (1997).
2. E. J. H. Collart, G. de Cock, A. J. Murrell, and M. A. Foad, *Mater. Res. Soc. Symp. Proc.,* **525**, 227 (1998).
3. D. F. Downey, S. D. Marcus, and J. W. Chow, *J. Electron. Mater.,* **27**, 1296 (1998).
4. J. Gelpey, K. Elliott, D. Camm, S. McCoy, J. Ross, D. F. Downey, and E. A. Arevalo, Abstract 735, The Electrochemical Society Meeting Abstracts, Vol. 2002-1, Philadelphia, PA May 12-17, 2002.
5. M. Y. L. Jung, R. Gunawan, R. D. Braatz, and E. G. Seebauer, *AIChE J.*, Submitted.
6. R. Gunawan, M. Y. L. Jung, R. D. Braatz, and E. G. Seebauer, *J. Electrochem. Soc.,* **150**, G758 (2003).
7. M. Y. L. Jung, R. Gunawan, R. D. Braatz, and E. G. Seebauer, *J. Electrochem. Soc.,* **150**, G758 (2003).
8. See M. Law, http://www.swamp.tec.ufl.edu/
9. H.-H. Vuong, C. S. Rafferty, S. A. Eshraghi, J. Ning, J. R. McMacken, S. Chaudhry, J. McKinley, and F. A. Stevie, *J. Vac. Sci. Technol. B,* **18**, 428 (2000).
10. M. Y. L. Jung, R. Gunawan, R. D. Braatz, and E. G. Seebauer, *J. Appl. Phys*., Submitted.
11. L. H. Zhang, K. S. Jones, P. H. Chi, and D. S. Simons, *Appl. Phys. Lett.,* **67**, 2025 (1995).
12. M. J. Caturla, M. Foad, and T. D. de la Rubia, in *Proceedings of the International Conference on Ion Implantation Technology*, Vol. 2, IEEE, p. 1018 (1999).
13. H. Kobayashi, I. Nomachi, S. Kusanagi, and F. Nishiyama, *Mater. Res. Soc. Symp. Proc.,* **669**, J 5.3 (2001).
14. D. F. Downey, S. W. Falk, A. F. Bertuch, and S. D. Marcus, *J. Electron. Mater.,* **28**, 1340 (1999).
15. G. Mannino, P. A. Stolk, N. E. B. Cowern, W. B. de Boer, A. G. Dirks, F. Roozeboom, J. G. M. van Berkum, P. H. Woerlee, and N. N. Toan, *Appl. Phys. Lett.,* **78**, 889 (2001).
16. A. Agarwal, H.-J. Gossmann, and A. T. Fiory, *J. Electron. Mater.,* **28**, 1333 (1999).
17. H.-H. Vuong, C. S. Rafferty, S. A. Eshraghi, J. Ning, J. R. McMacken, S. Chaudhry, J. McKinley, and F. A. Stevie, *J. Vac. Sci. Technol. B,* **18**, 428 (2000).
18. N. E. B. Cowern, G. F. A. van de Walle, D. J. Gravesteijn, and C. J. Vriezema, *Phys. Rev. Lett.,* **67**, 212 (1991); N. E. B. Cowern, G. F. A. van de Walle, P. C. Zalm, and D. J. Oostra, *Phys. Rev. Lett.,* **69**, 116 (1992).
19. C. S. Nichols, C. G. Van de Walle, and S. T. Pantelides, *Phys. Rev. B,* **40**, 5484 (1989).
20. E. G. Seebauer, *Surf. Sci.,* **316**, 391 (1994).
21. Z. Du, A. F. Sarofim, and J. L. Longwell, *Energy Fuels,* **4**, 296 (1990).
22. X.-Y. Liu, W. Windl, and M. P. Masquelier, *Appl. Phys. Lett.,* **77**, 2018 (2000).